2-1-2000

Enhancement of Air Jet Impingement Heat Transfer using Pin-Fin Heat Sinks

H A. El-Sheikh

S V. Garimella
Purdue Univ, sureshg@purdue.edu

Enhancement of Air Jet Impingement Heat Transfer Using Pin-Fin Heat Sinks

Hani A. El-Sheikh and Suresh V. Garimella

***Abstract*—The enhancement of heat transfer from a discrete heat source in confined air jet impingement was experimentally investigated. A variety of pin-fin heat sinks were mounted on the heat source and the resulting enhancement studied. Average heat transfer coefficients are presented for a range of jet Reynolds numbers ($8000 \leq \mathrm{Re} \leq 45000$) and orifice diameters ($12.7 \leq d \leq 38.1$ mm). A total fin effectiveness was computed for the pinned heat sinks relative to the unpinned ones, and was in the range of 2.4 to 9.2; the highest value was obtained for the largest nozzle diameter. Heat transfer rates from the bare heat source were increased by a factor of 7.5 to 72 due to the introduction of the heat sinks. Results for the average heat transfer coefficient were correlated in terms of Reynolds number, fluid properties and geometric parameters of the heat sinks.**

***Index Terms*—Air jets, confined jets, electronics cooling, enhancement, heat sinks, heat transfer, jet impingement, pin fins.**

NOMENCLATURE

A_{base}	Heat sink base area (footprint), m^2.
A_{chip}	Surface area of simulated chip, m^2.
A_d	Area of orifice ($\pi d^2/4$), m^2.
A_{HS}	Total exposed surface area of heat sink, m^2.
A_r	Area ratio defined as $4(1.9d)^2/D_e^2$ used in (4).
A_{rs}	Area ratio defined as $4d^2/D_e^2$ used in (5), (6).
C	Clearance above fin tips, m.
C_p	Specific heat of air, J/kg.K.
d	Orifice diameter, m.
D_e	Equivalent diameter of square heat sink base, m.
d_p	Pin fin diameter, m.
H	Nozzle-to-target spacing measured from heat sink base ($H_p + C$), m.
H_p	Pin height, m.
h_{base}	Heat transfer coefficient based on A_{base}, W/m^2·°C.
h_{HS}	Heat transfer coefficient based on A_{HS}, W/m^2·°C.
k	Thermal conductivity of air, W/m·°C.
l	Nozzle plate thickness, m.
Nu_{base}	Nusselt number ($h_{\mathrm{base}}d/k$).
Nu_{HS}	Nusselt number ($h_{\mathrm{HS}}d/k$).
Pr	Prandtl number ($\mu C_p/k$).
Q_{loss}	Heat losses, W.
Q_{tot}	Total heat input to heater assembly, W.
R_{cond}	Conduction/constriction thermal resistance, °C/W.
R	Convective thermal resistance, ($\equiv R_{bj}$), °C/W.
R_{int}	Thermal resistance of interface material, °C/W.
Re	Reynolds number ($U_j d/\nu$).
T_{base}	Area-averaged temperature of heat sink base,°C.
T_{jet}	Jet exit temperature,°C.
T_{chip}	Temperature of heat source surface,°C.
T_{riser}	Temperature at the bottom of the riser,°C.
T_∞	Ambient temperature,°C.
U_j	Jet exit velocity (Volume flow rate/orifice area), m/s.
ε_f	Total effectiveness of pin fins ($h_{\mathrm{base,pinned}}/h_{\mathrm{base,unpinned}}$).
μ	Dynamic viscosity of air, N·s/m^2.

Manuscript received February 9, 1999; revised February 29, 2000. This paper was recommended for publication by Associate Editor D. N. Donahoe upon evaluation of the reviewers' comments. This work was supported by Pycon, Inc., Santa Clara, CA.

H. A. El-Sheikh is with the Department of Mechanical Engineering, University of Wisconsin-Milwaukee, Milwaukee, WI 53201 USA.

S. V. Garimella is with the School of Mechanical Engineering, Purdue University, West Lafayette, IN 47907-1288 USA (e-mail: sureshg@ecn.purdue.edu).

Publisher Item Identifier S 1521-3331(00)04141-6.

I. INTRODUCTION

INCREASED miniaturization, higher power densities, and demands on system performance and reliability in electronic systems have necessitated more aggressive heat removal techniques in the thermal management of electronic components. Air jet impingement, especially in conjunction with surface enhancement, is an attractive option since heat-removal levels similar to liquid cooling may be achieved by this means.

The present study investigates the enhancement of heat transfer from discrete heat sources to axisymmetric, confined air jets. After impingement, the radial spread of air is confined in a channel bounded by the target surface and the nozzle plate, representative of the channels formed by stacks of circuit boards carrying electronic components. The orifice is square-edged and short, thus giving rise to a still-developing velocity profile.

Although a large number of studies on jet impingement have been reported, heat transfer from confined jets is not fully understood. In their studies of liquid jet impingement, Fitzgerald and Garimella [1] and Garimella and Rice [2] indicated that confinement of the impinging jet results in the formation of one or more recirculating toroidal patterns as the flow discharges along the target surface. Obot *et al*. [3] observed a reduction in local heat transfer coefficients on the order of 50% as a result of confining the air outflow. The effect of confinement is evident up to nozzle-to-target plate spacings of four to five nozzle diameters. San *et al*. [4] showed that the recirculating flow in confined jet impingement at high Reynolds numbers brings heated air back into the jet, thus degrading heat transfer in the stagnation region. This reduction in heat transfer was confirmed for liquid jets by Garimella and Rice [2].

The heat transfer coefficient under an impinging jet has a bell-shaped distribution with a maximum value at the stagnation point, followed by a decrease with radial distance from the

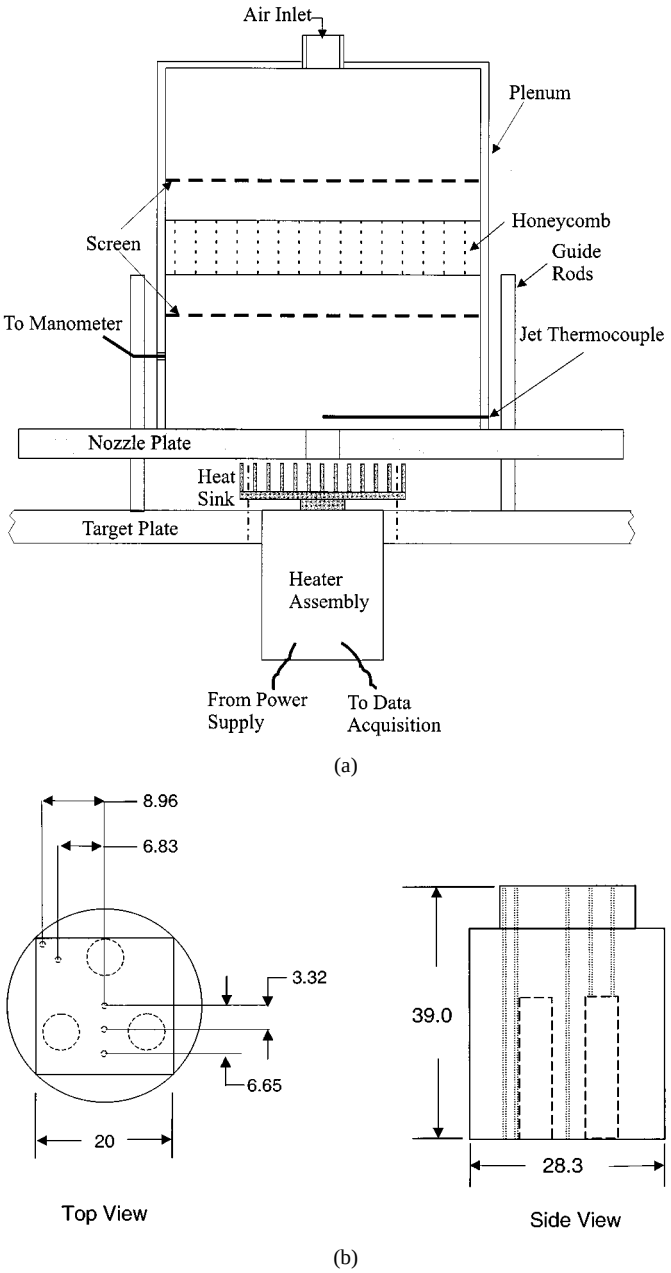

Fig. 1. (a) Schematic diagram of the test section of the air jet impingement facility. (b) Details of the copper block in the heat source assembly (all dimensions are in mm).

jet centerline. Secondary maxima have been reported at a radius of approximately $1.9d$ for circular jets in several studies (e.g., [2], [5], [6]). This secondary peak is generally understood to coincide with the location where the boundary layer becomes turbulent in the wall jet [7].

Although studies of jet impingement combined with surface modifications have shown good potential for enhanced heat transfer, limited information is available in the literature on such configurations. Hrycak [8] studied heat transfer from impinging air jets on a smooth plate with conical and ring protuberances; the cones gave rise to substantial increases in heat transfer ($\sim$60%), but the rings, in contrast, led to a reduction in local heat transfer rate. Hansen and Webb [9] considered air jet impingement on six different types of modified surfaces. They obtained enhancements in heat transfer relative to a smooth surface of 1.5 to 4.5 times. Sullivan *et al*. [10] studied the effect of using roughened spreader plates under circular liquid jets of FC-77, a perfluorinated dielectric liquid. Their study indicated that roughened spreader plates increase the heat transfer rate by 40% to 60% as compared to smooth plates. Also, higher heat transfer enhancements were obtained with the smaller-diameter nozzles. In a similar study by Priedeman *et al*. [11], liquid jets resulted in enhancement factors of 2.2 to 4.7 for FC-77, and 1.3 to 2.7 for water when modified surfaces were compared to unenhanced ones. Teuscher *et al*. [12] investigated FC-77 impingement on an array of discrete heat sources with pin fins and parallel-plate fins used as surface modifications. The former showed an increase in heat transfer coefficient by three times, while the parallel-plate fins resulted in a three to five times increase.

The present study is part of an ongoing research program which addresses extending the limits of air cooling in the thermal management of high-heat-flux electronic components. The heat transfer from discrete sources to single and multiple confined air jets was studied by Schroeder and Garimella [5], [13], while Brignoni and Garimella [14] presented results for optimizing the geometric dimensions and layout of single and multiple nozzles to maximize the performance of impingement on extended surfaces. In the present work, a variety of pin-fin heat sinks are evaluated when used in conjunction with confined impinging air jets, and the extent of heat transfer enhancement obtained is quantified. Generalized predictive correlations are proposed for the average heat transfer coefficients achieved in this arrangement.

II. Experimental Setup and Procedures

The experiments for the present work were conducted using the same facility as described in Schroeder and Garimella [5], [13]. Only salient details are provided here.

Air at ambient conditions is drawn into a variable-speed regenerative blower. The air flow rate is measured by one of three flow meters depending on the range, and delivered to a cylindrical plenum for flow conditioning, as shown in Fig. 1(a). Different plates containing orifices can be attached to the underside of the plenum. A pressure tap located on the plenum wall is used to measure pressure drop across the orifice, while a thermocouple measures the air temperature just upstream of the orifice. The jet issuing from the orifice plate impinges on a target plate which contains the heat source assembly. The nozzle-to-target plate spacing is set using three small high-precision gage blocks ($\pm 0.002\,54$ mm) in a triangular arrangement. Three different orifice plates were used in the experiments, with square-edged orifices of diameter $d = 12.7, 25.4$, and 38.1 mm.

The heater assembly consists of a cylindrical copper block, the upper part of which is machined down to a 20×20 mm square section, simulating a heat-generating electronic component. Three cartridge heaters are imbedded in the copper block as shown in Fig. 1(b). The copper block is surrounded by polypropylene insulation, leaving only the top surface of the square heat source exposed to the jet. The exposed heat source is mounted flush with the target plate. The surface temperature

TABLE I
DIFFERENT HEAT SINKS USED IN THE EXPERIMENTS

	Description	Base footprint, A_{base} (mm x mm)	Effective Surface area[§], A_{HS} (10^{-4} m^2)	Pin height, H_p (mm)	Pin diameter, d_p (mm)	Number of Pins	Pin Spacing (mm)	Pin Arrangement
Large pinned heat sinks (76.2x76.2 mm^2 footprint)	Short	76.2x76.2	371	12.7	1.6	540	2.9	Staggered
	Tall	76.2x76.2	747	25.4	1.6	540	2.9	Staggered
Small pinned heat sinks (50.8x50.8 mm^2 footprint)	Short	50.8x50.8	179	12.7	1.6	240	2.9	Staggered
	Short, fine pins	50.8x50.8	201	12.7	0.94	480	2.28	Staggered
	Tall	50.8x50.8	332	25.4	1.6	240	2.9	Staggered
Unpinned heat sinks (both footprints)	Large	76.2x76.2	58	0	-	0	0	N/A
	Small	50.8x50.8	26	0	-	0	0	N/A

[§] Includes surface area of pins and remaining footprint area of the base; i.e., side and bottom surface of the base not included.

of the heat source is determined as the arithmetic average of the readings from five 36-gage T-type thermocouples located just underneath the heat source surface [Fig. 1(b)].

Heat sinks can be mounted on top of the heat source using screws, with a thermally conductive pad (T-GON 805) used as the interface material. The clamping force was measured and maintained constant for all tests at approximately 45 lb. Seven copper pin-fin heat sinks, custom-made by Pin Fin, Inc., were studied in the experiments, as listed in Table I. The heat sinks consist of three parts: riser, base, and pin fins, as shown in Fig. 2. The riser, which is 20×20 mm square in cross section and 9.5 mm high, is brazed to the square heat sink base, and serves merely as a conduit for heat. Two sizes of heat sink footprint were considered: Small ($A_{\text{base}} = 50.8 \times 50.8$ mm^2) and Large ($A_{\text{base}} = 76.2 \times 76.2$ mm^2). The thickness of the heat sink base was held at 3.17 mm for all heat sinks. Pin fins of diameter $d_p = 1.6$ mm were studied at pin heights of $H_p = 25.4$ and 12.7 mm. A smaller pin diameter, $d_p = 0.94$ mm, was also considered. Two unpinned heat sinks (smooth base) were studied as a baseline.

Temperature measurements on the heat sinks were obtained at five different locations on the base of the sink and in the riser, as shown in Fig. 2. The riser temperature was measured at the center by a thermocouple positioned 1.52 mm from the bottom. The heat sink base temperature was measured at four different positions which are equally-spaced along the diagonal. The average heat sink base temperature, T_{base}, was obtained as a weighted area-average, the largest standard deviation being 3°C.

The voltage drop and current drawn by the cartridge heaters as well as all the thermocouple readings were logged by a Fluke NetDAQ data acquisition system. The measurements are made after steady state is reached, typically in about 45 min. for each test, and are averaged over 200 points. Of the total power input, the heat lost by conduction through the insulation was determined experimentally under no-flow conditions, using a procedure similar to that of Obot and Trabold [15]. From these no-flow experiments, an expression for heat loss was obtained as $Q_{\text{loss}}\,(\text{W}) = 0.0645\,(\text{W/°C}) \cdot (T_{\text{chip}} - T_{\infty})(\text{°C})$. This heat loss was subtracted from the total heat supplied to the chip under impingement conditions with $T_{\infty} \equiv T_{\text{jet}}$. The average heat transfer coefficient for the heat sinks was thus calculated according to

$$h_{\text{base}} = \frac{Q_{\text{tot}} - Q_{\text{loss}}}{A_{\text{base}}(T_{\text{base}} - T_{\text{jet}})} \tag{1}$$

An alternative definition of average heat transfer coefficient based on the total exposed heat sink area, A_{HS} (including the surface area of the pins), is also used in the results presented in this paper:

$$h_{\text{HS}} = \frac{Q_{\text{tot}} - Q_{\text{loss}}}{A_{\text{HS}}(T_{\text{base}} - T_{\text{jet}})} \tag{2}$$

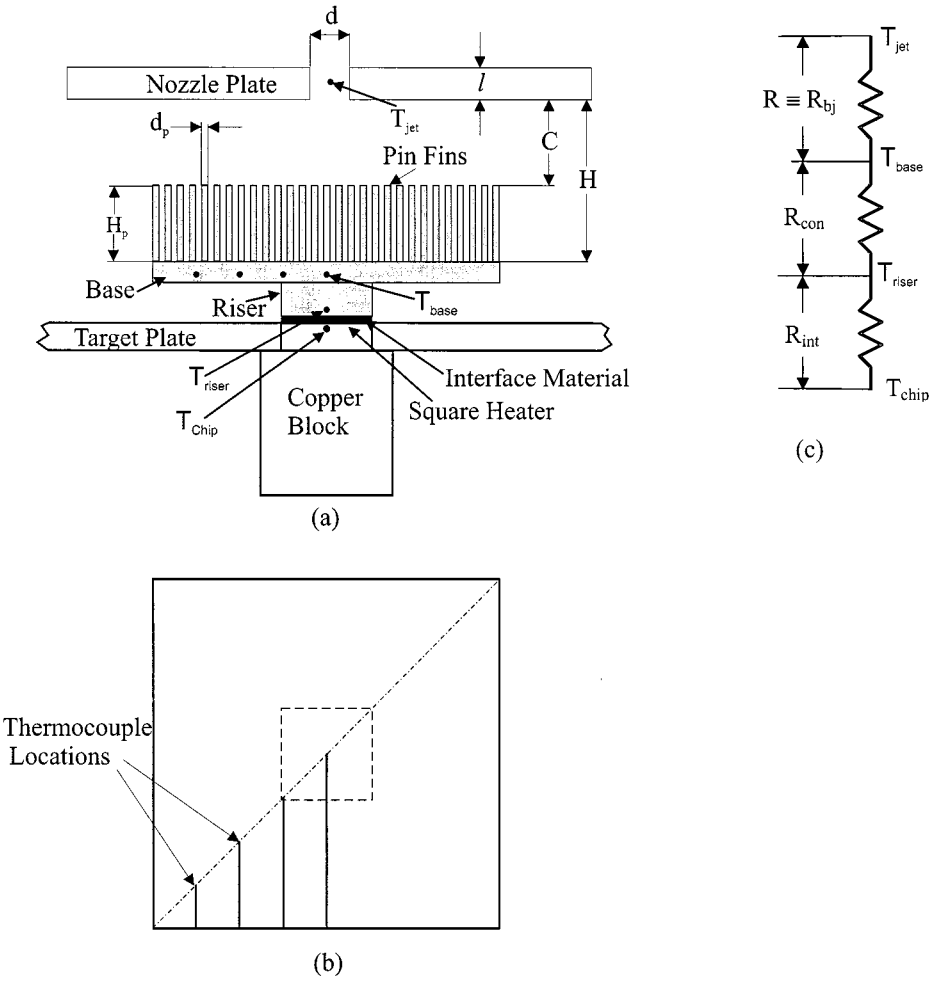

Fig. 2. Description of the heat sinks: (a) the pinned heat sink showing geometric parameters, (b) top view of the heat sink base showing thermocouple locations, and (c) thermal resistance diagram.

Thermal resistances (°C/W) may be calculated from these definitions using:

$$R = \frac{T_{\text{base}} - T_{\text{jet}}}{Q_{\text{tot}} - Q_{\text{loss}}} \tag{3}$$

It may be noted that the heat transfer coefficient in this study is always defined based on the temperature difference between the base of the heat sink and the jet. Thus, although the resistance of the interface material (R_{int}) is determined (from measured values of T_{chip} and T_{riser}), it is not factored into the discussion of results in this study.

A standard uncertainty analysis revealed uncertainties in the heat transfer coefficient of 3.4% to 10.2% with the maximum value resulting for the large heat sink at the highest flow rate. The largest contribution to uncertainty (89%) comes from uncertainties in temperature measurement (±0.3°C). The contribution from uncertainty in Q_{tot} was approximately 8%. Experiments performed over a period of months were found to have excellent repeatability.

III. Results and Discussion

Average heat transfer coefficients are presented in this section for the seven heat sinks investigated in the experiments. The effects on heat transfer of different geometric parameters of the heat sinks and jet flow conditions are explored. The heat transfer coefficients obtained with the pin-fin heat sinks are compared to the unpinned cases and the results are presented in the form of fin effectiveness under different jet flow rates and nozzle diameters. The measured pressure drop values for all three nozzles are presented as a function of flow rate to aid in design implementations. Correlating equations are then proposed for the heat transfer coefficients for all the unpinned and pinned heat sinks.

Exploratory tests to determine the effect of nozzle-to-target plate spacing (H/d) on the heat transfer coefficient for both pinned and unpinned heat sinks revealed only a modest dependence on H/d (data not shown). For instance, changing H/d from 1 to 3 caused a maximum increase in heat transfer coefficient of 8% for both the pinned and unpinned surfaces. Heindel *et al*. [16] also observed that for fully turbulent jets, the heat transfer at $H/d = 3$ slightly exceeds that at $H/d = 1$. In view of the small effect of H/d on heat transfer for the entire range of Reynolds number $(8000 \leq \text{Re} \leq 45\,000)$ and nozzle diameters considered in this study, a single clearance height, $C = 12.7$ mm, was set throughout the rest of the experiments.

Heat transfer coefficients for the small heat sinks (solid symbols in all figures) with the two different pin heights as well as

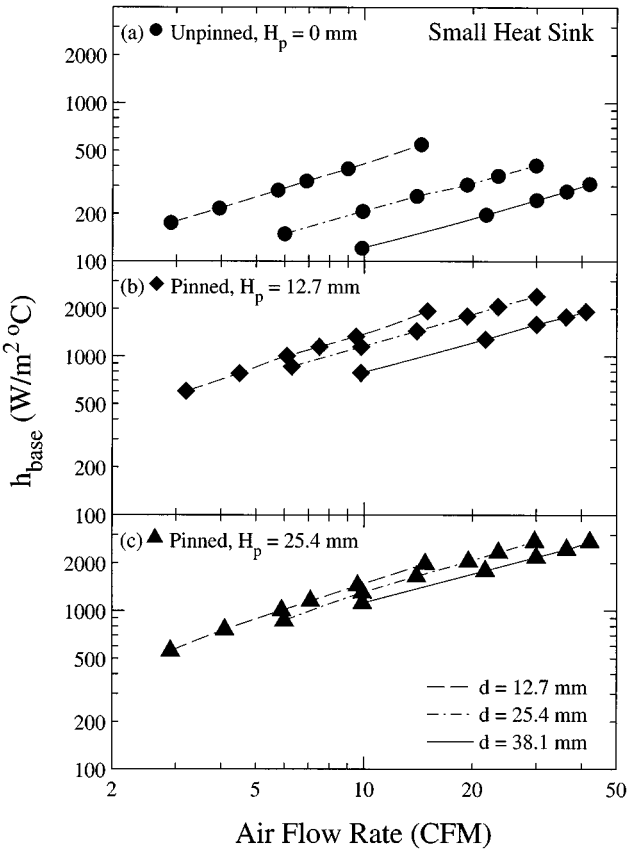

Fig. 3. Variation of heat transfer coefficient as a function of air flow rate with different nozzle diameters, for the small heat sinks.

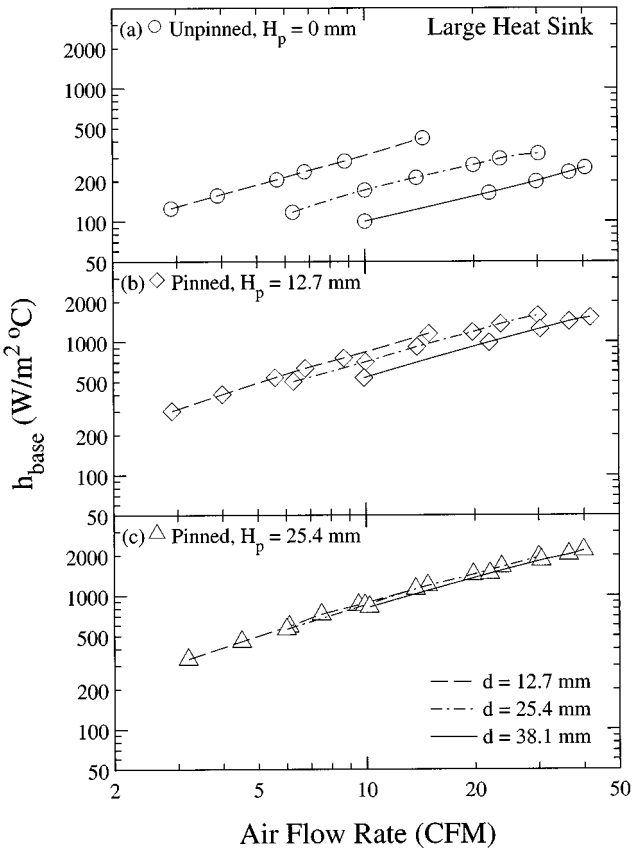

Fig. 4. Variation of heat transfer coefficient as a function of air flow rate with different nozzle diameters, for the large heat sinks.

the unpinned case are plotted in Fig. 3 as a function of air flow rate. For each heat sink, results for all three nozzle diameters are shown. In all cases, the heat transfer coefficient is seen to increase as the nozzle diameter decreases at a fixed flow rate. However, the influence of nozzle diameter is much more pronounced for the unpinned heat sink than for the pinned sinks. This trend of increases in heat transfer coefficients with a decrease in nozzle diameter is consistent with results for liquid jets in the literature [10], [16], and may be attributed merely to the increased jet exit velocity. However, this trend may not continue to be valid for nozzle diameters outside the range considered here; for instance, if much smaller diameters were used, the ratio of target surface area to the nozzle open area would be greatly increased, and the average heat transfer for a fixed target area may decrease with a decrease in nozzle diameter.

Similar results are shown for the unpinned and pinned large heat sinks (open symbols in all figures) in Fig. 4, again for all three nozzle diameters. As for the small heat sink, the heat transfer coefficient increases as nozzle diameter decreases, especially for the unpinned heat sink. However, the influence of nozzle diameter almost entirely vanishes for the taller pinned heat sink. It may be deduced that as the heat sink surface area increases, the effect of nozzle diameter diminishes; this point is further explored in the following discussion.

From the foregoing results, it emerges that the key factors governing heat transfer rates in confined jet impingement on heat sinks are the jet exit velocity and the total surface area of the heat sink. It may be inferred from the results that as the heat sink surface area is increased, a critical value is reached beyond which it overshadows the role of jet velocity. Thus, for the relatively large surface areas characterizing the large pinned heat sinks, changes in the nozzle diameter at a fixed flow rate (and the associated changes in jet velocity) have little or no effect on heat transfer, as demonstrated in Fig. 4.

However, it is also seen from the results that increasing the surface area of a heat sink with a given footprint by increasing the height of the pins leads to only modest gains in heat transfer coefficient. This is illustrated in Fig. 5, where the effect of pin height is investigated for the small and large heat sinks, for a fixed nozzle diameter of 12.7 mm. Two effects come into play in these results. On the one hand, the fin efficiency of each pin decreases as the pin height increases. However, since the pin fins in this study are made of copper, they retain most of the fin efficiency even as the pin height is increased from 12.7 mm to 25.4 mm, with the efficiency reducing from 98% to 80%. A second and more important effect is related to the details of the impingement flow field: the increase in pin height adds area in a region of low flow velocities, and hence does not add perceptibly to heat transfer. Thus, although the taller-pin heat sinks comprise almost twice the area of the shorter-pin counterparts, the heat transfer coefficients are only different by 5%. This is true for both the small and large heat sinks. Fig. 5 also shows that the small heat sink has a significantly higher (by 100%) heat transfer coefficient than the large heat sink. This is because more of the small heat sink is in the highly effective impingement region of the jet; a good part of the large heat sink is in the wall

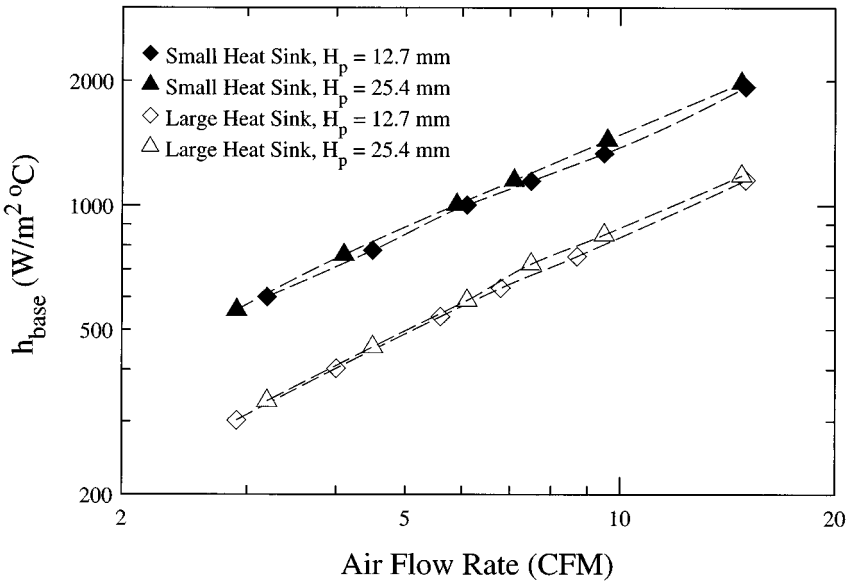

Fig. 5. Variation of heat transfer coefficient as a function of air flow rate for both the small and large heat sinks at two different pin heights, for a nozzle diameter of $d = 12.7$ mm.

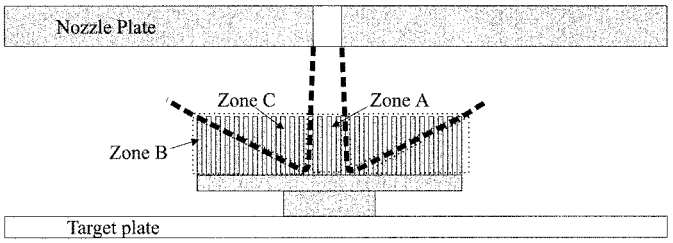

Fig. 6. Proposed zones in the confined impingement flow field.

jet region with the associated lower local heat transfer rates. In addition, since the heat source beneath the heat sinks (and the riser carrying this heat to the heat sinks) is significantly smaller in area (20 by 20 mm) than the heat sink base, the spreading resistance must be factored into an analysis of the heat sink performance. As the heat sink footprint is increased, more and more of its periphery is in a region into which heat from the riser does not spread. In addition, the impinging jet is most effective at heat removal in the impingement zone. The addition of heat transfer area far from this impingement zone would contribute little to enhanced heat transfer. In cases where higher heat removal rates are required, the large heat sinks could be used in conjunction with arrays of multiple jets to more evenly spread the impinging flow.

The mechanisms proposed above may be better understood by making reference to Fig. 6. The flow field in the confined region between the nozzle and target plates may be considered to consist of three zones as shown in the figure: zone A where the flow is parallel to the axis of the pins (the impingement zone); zone B where the jet is in crossflow past the pins (the "wall-jet" region); and zone C which is outside the "wall jet" and experiences low velocities and recirculating flow. With reference to the preceding discussion of the effect of pin height, it appears that increasing the pin height adds area primarily in zone C, and is thus not very effective at increasing heat transfer. In future work, these mechanisms will be verified using flow visualization and local flow field measurements.

The influence of one additional parameter of the pin fin heat sinks, the pin diameter, is explored in Fig. 7. Two different definitions of the heat transfer coefficient are used in the graph, $h_{\rm base}$ based on the heat sink base area $(A_{\rm base})$ and used in the figures thus far, and $h_{\rm HS}$ based on the total exposed area $(A_{\rm HS})$ of the heat sink. The rationale for using the latter definition lies in the high fin efficiencies of the copper pins used. The fin efficiency was never less than 80%, and thus, it is assumed that the entire heat sink area is active in heat transfer; no corrections are made in the calculation of total exposed area of the heat sink to account for fin efficiency. The figure shows results for two different pin diameters, 0.94 and 1.6 mm, for all three nozzle diameters tested. The convection coefficient $h_{\rm base}$ is higher for the smaller pin diameter; for example at roughly 10 CFM, the smaller pin diameter yields heat transfer coefficients that are higher by 25% for the largest nozzle diameter and 8% for the smallest. However, $h_{\rm HS}$ is only slightly affected by changes in pin diameter (the scales in the figure are logarithmic).

The total effectiveness of the pin fins is defined as $\varepsilon_f = (h_{\rm base,pinned}/h_{\rm base,unpinned})$, and plotted in Fig. 8 as a function of flow rate with different nozzle diameters for the three small heat sinks. The effectiveness decreases with decreasing nozzle diameter for a given flow rate. However, the effectiveness for any one heat sink does not vary appreciably with flow rate for the same nozzle diameter. For $d = 12.7$ mm, all three small heat sinks have effectiveness values in the range of 3.2 to 3.8, while for $d = 38.1$ mm, this range is from 6.2 to 9.2. Brignoni and Garimella [14] and Heindel *et al.* [16] also found that the large nozzle diameters resulted in greater effectiveness values. Also, the tall pins and the short fine pins provide higher effectiveness values. Similar results for effectiveness are shown in Fig. 9 for the large heat sinks, where the effectiveness is seen to range from 2.4 to 9.2, depending on the nozzle diameter and pin height.

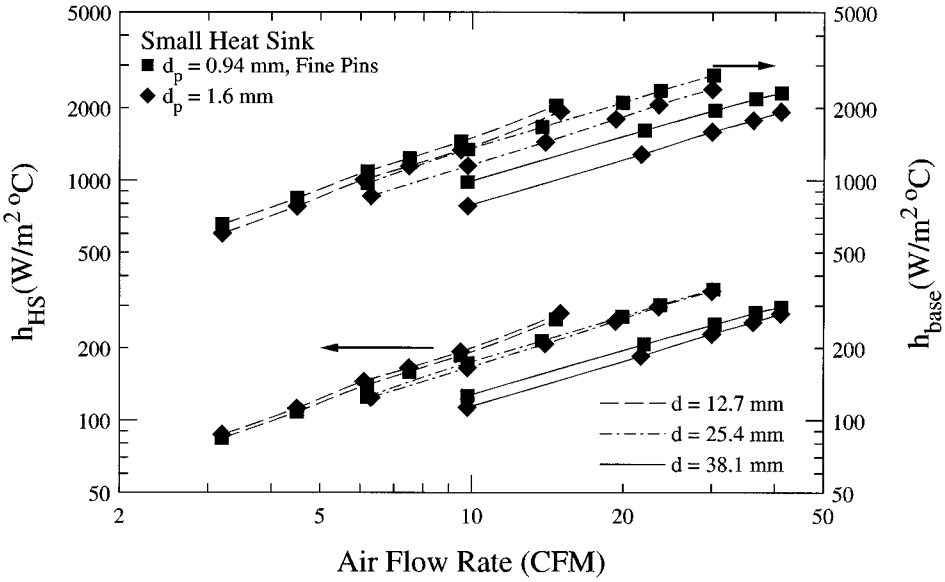

Fig. 7. Variation of heat transfer coefficient $(h_{\rm HS}, h_{\rm base})$ with air flow rate for different pin diameters with three different nozzles, for the small heat sinks; the upper group of six lines shows $h_{\rm base}$, while the lower group shows $h_{\rm HS}$. It may be noted that the scale is logarithmic.

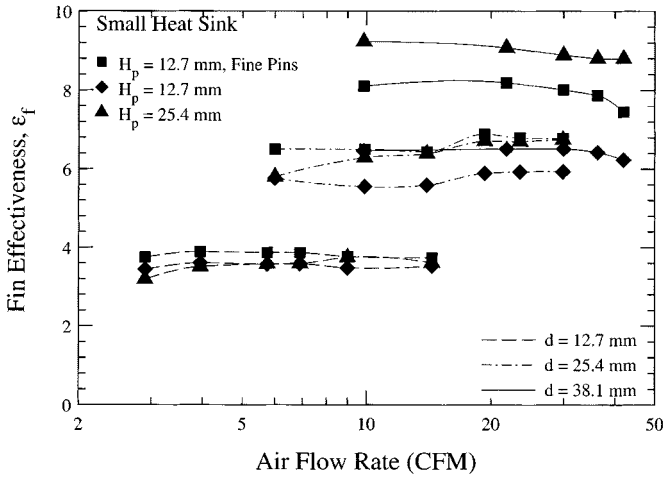

Fig. 8. Fin effectiveness as a function of air flow rate for all the small heat sinks.

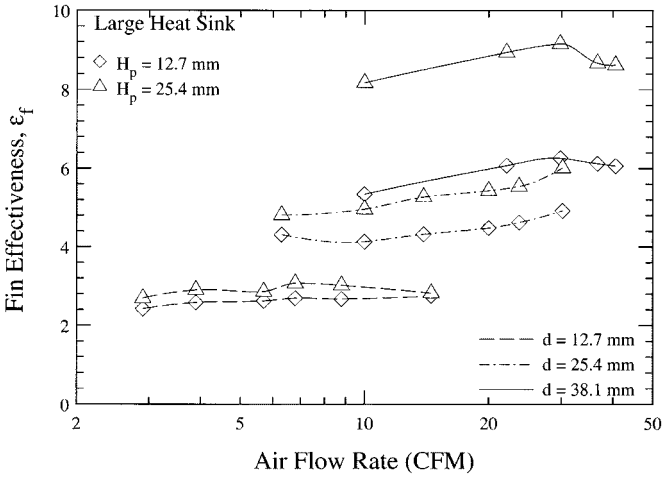

Fig. 9. Fin effectiveness as a function of air flow rate for all the large heat sinks.

While the fin effectiveness discussed above serves as a measure of the heat transfer enhancement effected by the fins compared to an unpinned surface, the overall enhancement in heat transfer due to the presence of the entire heat sink (riser, base and pins) is also of interest. This is captured by defining an enhancement factor as the ratio of heat removal rates with and without the heat sink in place under the same flow conditions; in the absence of the heat sink, only the 20×20 mm simulated chip is exposed to the impinging jet. It may be noted that this definition does not include the contribution of the (application-dependent) interface material resistance, which, if included, would result in reduced values for the enhancement factor. The enhancement factor obtained with the heat sinks used in this study ranged from a factor of 7.5 to 72 times relative to the bare surface; the lower end of this range was obtained for the small, unpinned heat sink while the upper end of the range was characteristic of the large, tall-pin heat sink.

To aid in practical design implementations of air jet impingement on heat sinks, Table II shows the pressure drop values for all three nozzles as a function of flow rate. Most of the pressure drop in this cooling technique occurs across the nozzle; this nozzle pressure drop overwhelms any contribution of the presence of the heat sink to pressure drop. In fact, no difference was observed in the measurements of pressure drop with and without the heat sink present for a given nozzle plate under the conditions of this test.

IV. Correlations

The heat transfer coefficients obtained in this study were correlated in terms of Nusselt number (hd/k), and resulted in different correlations for the unpinned and pinned heat sinks. The unpinned heat sink Nusselt numbers were found to be a function of the jet velocity (Re), the fluid properties (Pr), and equivalent diameter of the heat sink base (D_e) as in previous studies of confined air jet impingement [5], [13]. Following an approach previously used [5], [13], [16], the data were correlated as a combination of area-weighted contributions from

TABLE II
PRESSURE DROP ACROSS DIFFERENT NOZZLES TESTED

	Flow rate (CFM)	Reynolds number, Re	Pressure drop (kPa)
Nozzle Diameter d = 12.7 mm	2.9	8639	0.11
	4.1	12213	0.24
	5.9	17575	0.5
	7.1	21150	0.75
	9.6	28597	1.4
	14.8	44088	3.2
Nozzle Diameter d = 25.4 mm	6	8937	0.05
	9.9	14746	0.14
	14	20852	0.28
	19.5	29044	0.54
	23.6	35151	0.79
	29.7	44237	1.28
Nozzle Diameter d = 38.1 mm	9.9	9830	0.03
	21.7	21547	0.15
	30.	29789	0.29
	36.4	36144	0.43
	42.2	41903	0.6

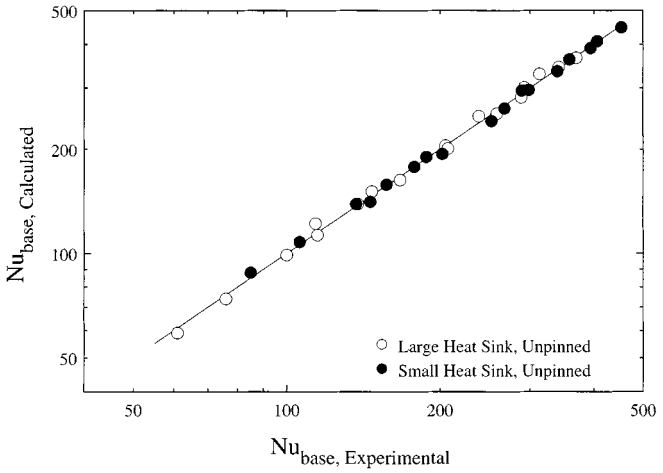

Fig. 10. Comparison between experimental and predicted [see (4)] results for $\mathrm{Nu_{base}}$ for the unpinned heat sinks.

the impingement ($0 \leq r \leq 1.9d$, [7]) and wall-jet regions ($r > 1.9d$). In the correlations the exponent for Prandtl number was fixed at 0.4 [2], [6] since it was not an independently varied parameter in this study.

A single correlation that predicts the Nusselt number ($\mathrm{Nu_{base}}$) for the unpinned heat sinks with average and maximum deviations from the experimental results of 2.1% and 6.7%, respectively, was

$$\mathrm{Nu_{base}} = 0.727\mathrm{Re}^{0.634}\mathrm{Pr}^{0.4}(D_e/d)^{-0.440}A_r + 0.035\mathrm{Re}^{0.877}\mathrm{Pr}^{0.4}(D_e/d)^{-0.321}(1-A_r). \quad (4)$$

If $A_r \geq 1$, it is set equal to 1. In this study, $A_r = 1$ for all but the smallest diameter nozzle. Equation (4) is valid for $8000 \leq \mathrm{Re} \leq 45000, 12.7 \leq d \leq 38.1$ mm and $0.08 \leq l/d \leq 1$. A plot of the calculated $\mathrm{Nu_{base}}$ as predicted by (4) versus the experimental values is presented in Fig. 10.

A similar approach was employed to arrive at a correlation for the Nusselt number when the pin fins were present, i.e., for all five pinned heat sinks and the three nozzle diameters studied. Correlations were obtained in terms of Nusselt numbers defined in two different ways: one for $\mathrm{Nu_{base}}$ based on the heat sink footprint area, and the other for $\mathrm{Nu_{HS}}$ based on the total heat sink surface area. The first of these correlations was:

$$\mathrm{Nu_{base}} = 7.953\mathrm{Re}^{0.621}\mathrm{Pr}^{0.4}(D_e/d)^{-0.968}A_{\mathrm{rs}} + 3.363\mathrm{Re}^{0.812}\mathrm{Pr}^{0.4}(D_e/d)^{-1.897}(1-A_{\mathrm{rs}}). \quad (5)$$

Again, if $A_{\mathrm{rs}} \geq 1$, it is set equal to 1. Equation (5) is valid for the same parameter ranges as (4). It may be noted that A_{rs} allots approximately a quarter of the area A_r to the impingement zone; data from the pinned heat sinks were more successfully correlated when A_{rs} was used in preference to A_r used in (4). This equation represents the experimental results for all the pinned heat sinks at all three nozzle diameters with average and maximum deviations of 9.8% and 24%, respectively, as shown in Fig. 11. An alternative correlation, in terms of $\mathrm{Nu_{HS}}$, was

$$\mathrm{Nu_{HS}} = 2.759\mathrm{Re}^{0.620}\mathrm{Pr}^{0.4}(A_{\mathrm{HS}}/A_d)^{-0.536}(D_e/d)^{0.217}A_{\mathrm{rs}} + 2.083\mathrm{Re}^{0.817}\mathrm{Pr}^{0.4}(A_{\mathrm{HS}}/A_d)^{-0.928} \times (D_e/d)^{-0.114}(1-A_{\mathrm{rs}}). \quad (6)$$

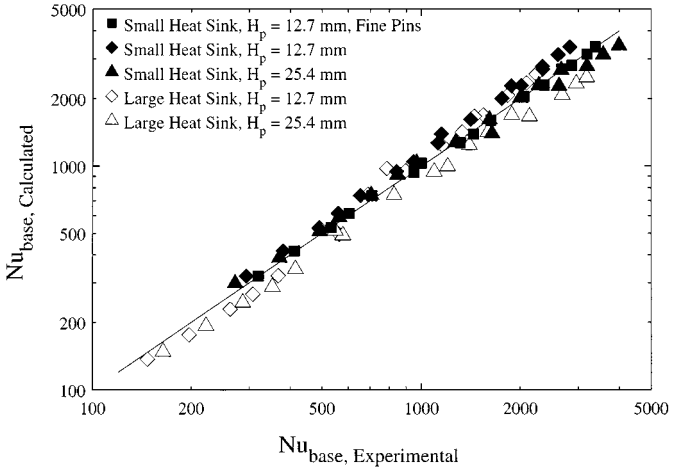

Fig. 11. Comparison between experimental and predicted [see (5)] results for $\mathrm{Nu_{base}}$ for the pinned heat sinks.

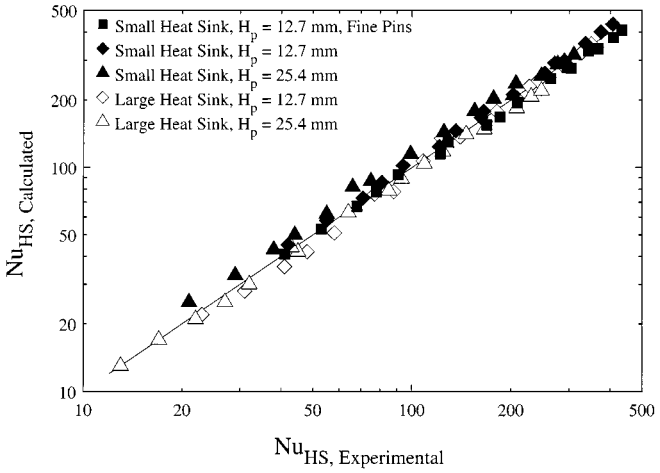

Fig. 12. Comparison between experimental and predicted [see (6)] results for $\mathrm{Nu_{HS}}$ for the pinned heat sinks.

The average deviation from experimental data of predictions with (6) is improved to 6.6%. A plot of Nusselt numbers calculated from (6) versus experimental data is shown in Fig. 12. The agreement in Figs. 11 and 12 between the predicted and experimental results is quite satisfactory in view of the wide range of parameters represented.

V. Conclusion

Experimental results were obtained for the heat transfer obtained in confined air jet impingement on a square heat source to which heat sinks are attached. Five pin-finned heat sink assemblies with different pin heights, pin diameters and footprint areas were studied and compared to two baseline, unpinned heat sinks at different nozzle diameters as a function of air flow rate. At a fixed flow rate, a decrease in nozzle diameter resulted in an improvement in heat transfer; however, the effect of nozzle diameter was much more pronounced for the unpinned heat sinks. The competing effects of jet velocity and heat sink surface area in determining the heat transfer from the heat sink are discussed in terms of three zones in the confined flow field delineated based on the extent and direction of flow in each zone. Smaller pin diameters showed higher heat transfer coefficients, by 8 to 25% depending on the nozzle diameter. The enhancement in heat transfer was found to be a strong function of nozzle diameter and heat sink footprint area; at a given flow rate, the effectiveness decreases with decreasing nozzle diameter. The effectiveness of the pin-finned heat sinks, defined relative to the unpinned ones, was in the range of 2.4 to 9.2, with the upper end being achieved for the tall pins with the largest nozzle diameter. When compared to the bare heat source with no heat sink attached, the presence of the heat sink led to heat transfer increases by a factor of 7.5 (unpinned small heat sink) to 72 (large heat sink with tall pin fins). Pressure drop measurements are reported for all cases. Correlations are proposed for the heat transfer from the unpinned and pinned heat sinks in terms of flow rate and geometric parameters of the heat sinks and the nozzles.

Acknowledgment

The authors would like to thank V. Schroeder for his support.

References

[1] J. A. Fitzgerald and S. V. Garimella, "Visualization of the flow field in a confined and submerged impinging jet," *ASME HTD*, vol. 346, no. 8, pp. 93–99, 1997.
[2] S. V. Garimella and R. A. Rice, "Confined and submerged liquid jet impingement heat transfer," *J. Heat Transf.*, vol. 117, pp. 871–877, 1995.
[3] N. T. Obot, W. J. Douglas, and A. S. Mujumdar, "Effect of semi-confinement on impingement heat transfer," in *Proc. 7th Int. Heat Transf. Conf.*, vol. 3, 1982, pp. 394–400.
[4] J.-Y. San, C.-H. Huang, and M.-H. Shu, "Impingement cooling of a confined circular air jet," *Int. J. Heat Mass Transf.*, vol. 40, pp. 1355–1364, 1997.
[5] V. P. Schroeder and S. V. Garimella, "Heat transfer from a discrete heat source in confined air jet impingement," in *Proc. 11th Int. Heat Transf. Conf.*, vol. 5, 1998, pp. 451–456.
[6] H. Sun, C. F. Ma, and W. Nakayama, "Local characteristics of convective heat transfer from simulated microelectronic chips to impinging submerged round water jets," *J. Electron. Packag.*, vol. 115, pp. 71–77, 1993.
[7] H. Martin, "Heat and mass transfer between impinging gas jets and solid surfaces," *Adv. Heat Transf.*, vol. 13, pp. 1–60, 1977.
[8] P. Hrycak, "Heat transfer from impinging jets to a flat plate with conical and ring protuberances," *Int. J. Heat Mass Transf.*, vol. 27, pp. 2145–2154, 1984.
[9] L. G. Hansen and B. W. Webb, "Air jet impingement heat transfer from modified surfaces," *Int. J. Heat Mass Transf.*, vol. 36, pp. 989–997, 1992.
[10] P. F. Sullivan, S. Ramadhyani, and F. P. Incropera, "Use of smooth and roughened spreader plates to enhance impingement cooling of small heat sources with single circular liquid jets," *Topics Heat Transf., ASME HTD*, vol. 206-2, pp. 103–110, 1992.
[11] D. Priedeman, V. Callahan, and B. W. Webb, "Enhanced surface liquid jet impingement heat transfer," *Enhanced Cooling Techn. Electron. Appl., ASME HTD*, vol. 263, pp. 43–48, 1993.
[12] K. L. Teuscher, S. Ramadhyani, and F. P. Incropera, "Jet impingement cooling of an array of discrete heat sources with extended surfaces," *Enhanced Cooling Techn. Electron. Appl., ASME HTD*, vol. 263, pp. 1–10, 1993.
[13] V. P. Schroeder and S. V. Garimella, "Heat transfer in confined multiple air-jet impingement," *Proc. ASME Heat Transf. Div.*, vol. 361-1, pp. 183–190, Nov. 1998.
[14] L. A. Brignoni and S. V. Garimella, "Experimental optimization of confined air jet impingement on a pin fin heat sink," *IEEE Trans. Comp. Packag. Technol.*, vol. 22, pp. 399–404, 1999.
[15] N. T. Obot and T. A. Trabold, "Impingement heat transfer within arrays of circular jets: Part 1—Effects of minimum, intermediate, and complete crossflow for small and large spacings," *J. Heat Transf.*, vol. 109, pp. 872–879, 1987.
[16] T. J. Heindel, S. Ramadhyani, F. P. Incropera, and A. Campo, "Surface enhancement of a heat source exposed to a circular liquid jet with annular collection of the spent fluid," *Topics Heat Transf.*, vol. 206-2, pp. 111–118, 1992. ASME HTD.

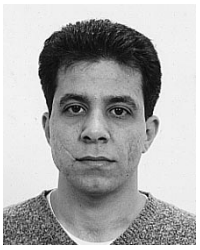

Hani A. El-Sheikh received the B.S. degree from United Arab Emirates University, United Arab Emirates, in 1993 and the M.S. degree from the University of Wisconsin, Milwaukee, in 1999, both in mechanical engineering.

He is a Thermal Engineering in the Research and Development Department, Pycon, Inc., Santa Clara, CA. His current work involves thermal management of high-power, next generation chips during burn-in and test.

Suresh V. Garimella received the B.Tech. degree from the Indian Institute of Technology, Madras, the M.S. degree from The Ohio State University, Columbus, and the Ph.D. degree from the University of California, Berkeley.

He is and Associate Professor in the School of Mechanical Engineering, Purdue University, West Lafayette, IN, prior to which he was Cray-Research Professor of Mechanical Engineering, University of Wisconsin, Milwaukee. He is Director of the Electronics Cooling Laboratory and has recently established the Cooling Technologies Research Consortium (http://widget.ecn.purdue.edu/~CTRC) to serve industry needs in the area of high-performance electronics packaging. His research interests also include crystal growth of electronic materials. He has published eighty technical papers in archival journals and conference proceedings, and has also contributed to, and edited, several books. He is on the Editorial Board of *Experimental Thermal and Fluid Science*.

Dr. Garimella received the Graduate School/UWM Foundation Research Award in recognition of outstanding research and creative activity in 1995, the UWM Distinguished Teaching Award in recognition of demonstrated dedication to excellence in undergraduate instruction in 1997, and the Society of Automotive Engineers' Ralph R. Teetor Educational Award in 1992. He is a member of the K-16 (heat transfer in electronic equipment) Committee, Heat Transfer Division, ASME.